Acetate ion augmented fluorescence sensing of Zn^{2+} by Salen-based probe, AIE character, and application for picric acid detection

Bhriguram Das[1,2] 🆔 | **Malay Dolai**[3] | **Anamika Dhara**[4] | **Subhabrata Mabhai**[5] |
Atanu Jana[6] | **Satyajit Dey**[2] | **Ajay Misra**[1]

[1] Department of Chemistry, Vidyasagar University, Midnapore, West Bengal 721102, India

[2] Department of Chemistry, Tamralipta Mahavidyalaya, Purba Medinipur, West Bengal 721636, India

[3] Department of Chemistry, Prabhat Kumar College, Contai 721404, India

[4] Department of Chemistry, Hiralal Mazumdar Memorial College For Women, Dakshineswar, North 24 Parganas, Kolkata 700035, India

[5] Department of Chemistry, Mahishadal Raj College, Mahishadal 721628, India

[6] Division of Physics and Semiconductor Science, Dongguk University, Seoul 04620, South Korea

Correspondence

Ajay Misra, Department of Chemistry , Vidyasagar University, Midnapore-721102, West Bengal, India.
Email: ajay@mail.vidyasagar.ac.in, ajaymsr@yahoo.co.in
Satyajit Dey, Department of Chemistry, Tamralipta Mahavidyalaya, Purba Medinipur, West Bengal. 721636.
Email: satyajitdeyoc@gmail.com
Atanu Jana, Division of Physics and Semiconductor Science, Dongguk University, Seoul, 04620, South Korea.
Email: atanujanaic@gmail.com

Funding information
University Grants Commission, Grant/Award Number: Sanction letter No. PSW-155/14-15(ERO) ID No. WV6-027

Abstract

Counter anion-triggered metal ion detection has been rarely reported by fluorimetric method. To address this challenging issue, a fluorescent probe ($\mathbf{H_2L}$) has been synthesized from bromo-salicylaldehyde and hydrazine hydrate, and structurally characterized by single crystal X-ray diffraction. The probe shows very weak fluorescence itself. However, its emission intensity increases in the presence of Zn^{2+} over other metal ions. Surprisingly, the emission profile of this probe in presence of Zn^{2+} is augmented only when acetate anion (OAcŕ) is present as counter anion, that allows for precise quantitative analysis by spectroscopic studies. The compositions and complexation among the probe, Zn^{2+} ion, and OAcŕ are supported by ESI-MS, ^{1}H-NMR, and Job's plot. Based on these studies, it is confirmed that the binding ratio between probe: metal is 1:2 and the detection limit (LOD) for the Zn^{2+} is 2.18 µM. The probe is capable of recognizing Zn^{2+} ion in the wide range of pH~6.5-9.5, and it could be efficiently recycled by EDTA. Furthermore, the combinatorial molecular logic gate and memory device have been constructed from the fluorescent behavior of $\mathbf{H_2L}$ with Zn^{2+}, OAcŕ, and EDTA input as based on NOT and AND gates. Interestingly, the aggregation-induced emission (AIEE) phenomenon is also perceived with greater than 50% water content in organic water mixtures, which are then useful for the detection of picric acid often used as explosive.

KEYWORDS
AIEE, counter anion, molecular logic gate, PET and CHEF, Picric acid, Schiff base, zinc sensor

1 | INTRODUCTION

Performing multiple tasks useful material is a significant and developing field of science in the cutting edge world. Such kind of materials makes an item modest, easy to use, and the time executives issue provides an endeavor and influence towards sustainable developments.[1,2] Schiff base is a reasonable example of such type of materials because of its versatile application in different field of applied science including medicine and pharmacy (viz., antifungal, antibacterial, biocidal, antitumor, antiviral, and antimalarial properties), chemical synthesis

448 | **Analytical Science Advances**

Full Article
doi.org/10.1002/ansa.202000165

Chemistry Europe
European Chemical
Societies Publishing

and analysis, modern imaging technologies, molecular memory storage, photochromic materials and photodetectors in biological systems, and in colorimetric and fluorimetric ion/ molecule sensors.[3–5] With that, the sensing of ions / small molecules by Schiff base has useful application in several interdisciplinary science like chemistry-biology, chemistry-physics, chemistry- mathematics, etc. due to its facile synthesis, superb selectivity and swift sensibility, exclusion of large instrument and huge cost unlike other several methods like atomic absorption spectroscopy (AAS), electrothermal atomization, inductively coupled plasma mass spectrometry, LC-GC/MS, solid-phase extraction (SPE), etc. Among the various metal ions present in the biosphere, Zn^{2+} is an important metal ion due to their direct and indirect involvement with the living species.[6,7] Zinc, the second most abundant transition element in human body after iron, fills in as an extra flagging job in the Central Nervous System (CNS), keeps up the auxiliary uprightness of proteins, and regulates gene expression.[8–10] Micronutrient zinc inadequacy can provoke cognitive weak, immune dysfunction, diarrhea and up to death especially in children.[11] Despite the fact that at low levels of zinc (76 μM in drinking water) is essential for cell function, amassing at more significant level zinc poisonousness prompts cardiovascular, reproductive, immune, and respiratory issues.[12–14] Along these lines, discovery and improvement of new class fluorescent sensors of Zn^{2+} is a significant assignment for researchers. However, as Zn^{2+} and Cd^{2+} are the isosteres have similar photophysical properties, discrimination of Zn^{2+} from Cd^{2+} is a challenging task.[15] Although there are many highly effective sensors for labile Zn^{2+}, most of them often need laborious multistep organic synthesis, which slows down the process of the invention and lead to very high costs and against the principle of a green approach. Furthermore, acetate ion is a critical component of numerous metabolic processes.[16,17] This anion is a possible tracer for malignancies and has been extensively investigated in prostate cancer and its metastases.[18]

Further, aggregation-induced emission (AIE) is an important and emerging scientific phenomenon of Schiff base molecule started distinctly on earlier decade by the pioneer Prof. B.Z.Tang.[19] In recent times, a number of organic luminogens display feeble emission in dilute solutions and become strong emissive in aggregated/solid-state.[20] Molecule demonstrating fluorescence in aggregate or solid state has enormous application in opto-electronic gadget like OLED and in cutting edge innovation.[21–24] Side by side, AIE phenomenon is a ready and enormous applied technique for nitroexplosive detection via fluorescence quenching.[25,26]

In this connection, number of reports in literature on AIE property of salen based Schiff base.[27–30] Zn^{2+} sensing with AIE property on salen derivative also reported.[31,32] However, the anion viz., acetate triggered Zn^{2+} sensing by Salen type Schiff base are rarely reported.[33,34]

Herein, we introduce a Schiff base fluorescent sensor [2,2′-((1E,1′E)-hydrazine-1,2 diylidenebis(methanylylidene))bis(4-bromo phenol)], H_2L for Zn^{2+}, derived from bromo-salicylaldehyde moiety which nearly covers all these requirements for Zn^{2+} over coexisting metal cations in a DMSO-water medium via a "turn on" signaling response assisted by only OAcŕ with ∼ 54 times emission intensity increment. Our as-synthesized chemosensor H_2L is the example of chemosensor for simultaneous detection of Zn^{2+} and OAcŕ ions in

a co-operative fashion. The reversible sensing features enables us to construct an advanced level three input (Zn^{2+}, OAcŕ and EDTA) single output molecular logic gate and molecular memory device. Simultaneously, by utilizing the benefit of AIE feature of H_2L, it has been applied as a fast, simple, and economically practical fluorescent chemosensor for picric acid detection in mixed aqueous media as well as in paper strips through immediate naked eye on site recognition.

2 | EXPERIMENTAL SECTION

2.1 | Materials and Methods

All the chemicals used throughout the study were acquired from the commercial suppliers. 5-bromosalicyladehyde (≥99.0%), hydrazine hydrate (>99.0%), methanol (≥99.0%), HEPES (99.0%), Na_2EDTA (98.0%), and glycerin were received from Merck India Ltd. Solvents used for spectroscopic studies were of analytical grade and distilled prior to their use. The progress of reaction monitored by TLC plate (F_{254}) obtained from Merck India LTD. Instruments used for: Locally made melting point apparatus for melting point measurements, Bruker 400 MHz instruments for NMR spectra acquire, QTOF mass spectrometer for ESI-MS, Perkin Elmer -100 FT-IR spectrometers for IR spectral collection, HORIBA Jobin Yvon Fluorocube-01-NL fluorescence lifetime spectrometer for lifetime measuring. The stock solutions of different metal ions were made either from perchlorate, chloride, acetate or nitrate salts in methanol or water. The stock solutions of different anions were made from respective sodium, or potassium salts. Double beam UV-Visible spectrometer (model-evolution 201) and Jasco 8500 fluorimeter were used for absorbance and fluorescence data acquisition, respectively.

2.2 | Single crystal X-ray crystallography

The data based on single crystal X-ray diffraction of H_2L was recorded (∼293K) on Bruker SMART APEX-III CCD diffractometer by graphite monochromated Mo-Kα radiation ($\lambda = 0.71073$Å). Bruker Apex-II suite was used to perform the data reduction, structure solution, refinement, and the integration of data by SAINT[35] program and the absorption corrections using SADABS.[35] SHELXL-2014[36] on F^2 is employed for full-matrix least-squares refinements using anisotropic refinement for all non-hydrogen atoms. All the hydrogen atoms become in their own geometrical places. The ORTEP vision is in Figure S1. The refinement data for H_2L is given in Table 1.

2.3 | Synthesis of the chemosensor H_2L

To the methanolic solution of 5-bromosalicyladehyde (201 mg, 1.0 mmol), hydrazine hydrate (25 mg, 0.5 mmol) in methanol was added dropwise with continuous stirring. The reaction was monitored by TLC plate from time to time. Further stirring for another 24 hrs gave a yellow colored precipitate. The ensuing product was collected, filtered, and recrystallized from methanol to obtain a bright yellow crystalline

449 **Analytical Science Advances**

Full Article
doi.org/10.1002/ansa.202000165

Chemistry Europe
European Chemical
Societies Publishing

TABLE 1 Crystal data and structure refinement for H_2L (CCDC No. 1961337)

Parameters	H_2L
Formula	$C_{14} H_{10} Br_2 N_2 O_2$
Formula Weight	398.04
Crystal System	triclinic
Space group	P -1
a, b, c [Å]	4.214(2), 13.778(8), 14.017(8)
α, β, γ [°]	61.226(5), 88.895(6), 88.396(6)
V [Å^3]	713.1(7)
Z	2
D (calc) [g/cm^3]	1.854
μ (MoK$_\alpha$) [/mm]	5.685
F (000)	388
Temperature (K)	293
Radiation [λ, Å]	0.71073
Theta Min-Max [°]	2.9, 26.4
Dataset	-5: 5; -17: 17; -17: 17
Tot., Uniq.Data, R(int)	4141, 1961, 0.042
Observed data [I > 2σ(I)]	1251
N_{ref}, N_{par}	1961, 183
R, wR_2, S	0.0504, 0.1508, 0.78
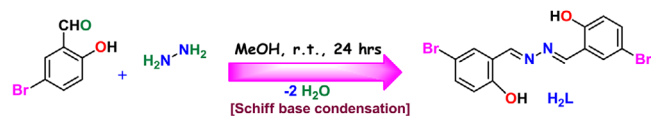
SCHEME 1 Synthetic route of the chemosensor H_2L

solid H_2L (Scheme 1). Yield: 93%, M.Pt.- 306-308°C (Lit. M.Pt.-303-305 °C). Elemental analysis: $C_{14}H_{10}Br_2N_2O_2$ Found (%): C, 42.61; H, 2.52; Br, 40.18; N, 7.02; O, 8.67. Calcd (%): C, 42.24; H, 2.53; Br, 40.15; N, 7.04; O, 8.04 ^{1}H NMR (500 MHz, DMSO-d6) (Figure S2) δ 11.13 (s, 2H), 8.94 (s, 2H), 7.90 (d, J = 2.3 Hz, 2H), 7.54 (dd, J = 8.7, 2.3 Hz, 4H), 6.95 (d, J = 8.8 Hz, 2H). ^{13}C NMR (125 MHz, DMSO-d6) (Figure S3) δ δ 161.22 (a), 158.15 (b), 135.62 (c),132.04 (d), 121.07 (e), 119.41 (f), 111.05 (g), MS-ESI+(m/z): [M+H]+, (Figure S4) Calculated: 397.91, Found: 397.8; FT-IR (KBr, cm-1) (Figure S5) 3562.5 (O-H), 1566.9 (-C = N-).

2.4 | Sample preparation for absorbance and photoluminescence studies

Stock solutions of various metal ions (1×10^{-2} mL^{-1}) were prepared in de-ionized water. A stock solution of H_2L (2×10^{-3} M) was prepared in DMSO-H_2O (9:1). The solution of H_2L was then diluted to 10×10^{-6} M with DMSO /aqueous HEPES buffer (5µM, pH 7.2; 9:1, v/v) for spectral studies by taking only 20 µL stock solution of H_2L (1×10^{-3} M) and making the final volume 2 mL adding DMSO. In selectivity experiments,

50 µL (1×10^{-2} M) metal ion or anion solution were added into 2 mL of H_2L solution (10×10^{-6} M). For fluorescence measurements, excitation wavelength was provided at 410 nm.

2.5 | Calculations of the detection limit

The detection limit is determined based on the fluorescence titration. The detection limit (LOD) of the probe H_2L for Zn^{2+} is determined using the following equation.[37]

$$Detection\ limit\ (LOD) = 3\sigma/k \tag{1}$$

where σ and k are the standard deviation of blank measurement and slope between the fluorescence emission intensity versus metal ion concentration, respectively.

2.6 | Binding constant evaluation

The binding constant (Ka) for the H_2L –Zn^{2+} complex was calculated using the following Benesi–Hildebrand equations from fluorescence titration data[38,39]

$$\frac{(F_{max} - F_0)}{(F - F_0)} = 1 + \frac{1}{K[Zn2+]^2} \tag{2}$$

where F_0, F, and F_{max} are the fluorescence intensity of H_2L in the absence of externally added Zn^{2+}, at different Zn^{2+} and with Zn^{2+} in large excess concentration, respectively. K (M^{-2}) is the association constant.

2.7 | Fluorescence lifetime measurements

Fluorescence lifetimes were determined by the method of Time-Correlated Single- Photon Counting (TCSPC). Laser diode at 375 nm was utilized as the excitation source and the signals were collected at the magic angle of 54.7° to eliminate fluorescence anisotropy decay. DAS-6 decay analysis programming was used for decay analysis. Mean (average) fluorescence lifetimes were measured using the following equation[40]

$$\tau_{av} = \frac{\sum \alpha_i \tau_i^2}{\sum \alpha_i \tau_i} \tag{3}$$

in which α_i is the pre-exponential factor corresponding to the ith decay time constant, τ_i.

2.8 | Computational details

The geometry optimizations of ligand (H_2L) and complex $[Zn_2(L)(OAc)_2]$(**1**) were generated in ground-state calculations and in

450 | **Analytical Science Advances**

Full Article
doi.org/10.1002/ansa.202000165

Chemistry Europe
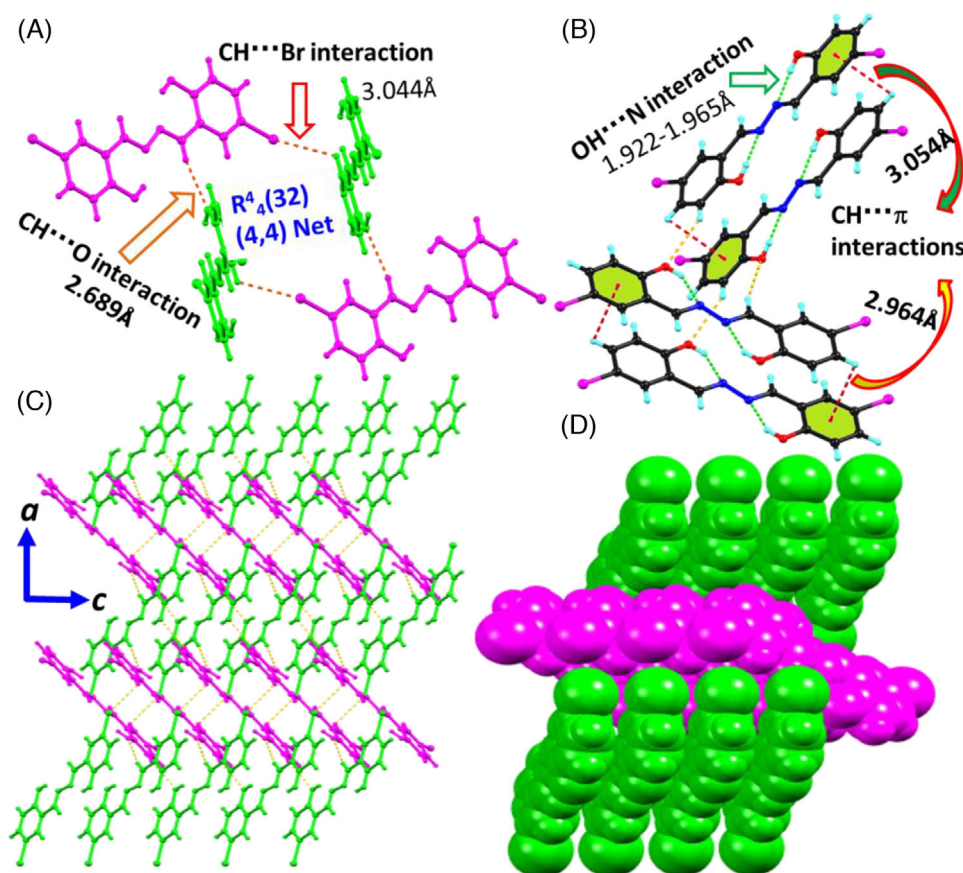European Chemical
Societies Publishing

FIGURE 1 In the picture the two molecules built from the two independent units are indicated in different colors: **A**, The H-bonded (4,4) net with molecular synthon $R^4_4(32)$; **B**, The molecular assemblies e.g. CH•••π and NH•••O interactions; **C**, The H-bonded 2D network in crystallographic ac plane; **D**, The space filling of crystal packing viewed down crystallographic "c" axis

the gas phase by DFT[41] method along with CPCM model (conductor-like polarizable continuum model).[42–44] B3LYP[45,46] function was employed for the study. The absorbance profile in DMSO medium for H_2L and $[Zn_2(L)(OAc)_2]$(**1**), were demonstrated by time-dependent density functional theory (TDDFT)[47] and used the lowest 40 singlet – singlet transitions for these calculations.

The 6-31+g basis set for C, H, N, O, and Zn atoms were employed for all the calculations. The frontier molecular orbitals with electron-density plots were arranged using Gauss View 5.1 software and Gaussian 09W software package.[48] Gauss Sum 2.1 program[49] was introduced to analyze the molecular orbital contributions.

3 | RESULTS AND DISCUSSION

3.1 | Synthesis of the chemosensor H_2L

The H_2L was prepared by a simple condensation reaction between hydrazine and 5-bromosalicyldehyde. The structure of H_2L was characterized by elemental analysis, SCXRD,[I]H & ^{13}C NMR, ESI-MS, FTIR spectroscopy (Figure S1-S5). The SEM-morphology of H_2L exhibits a rod-like shape (Figure 7).

3.2 | Structural description of H_2L

The ^{1}H NMR spectrum of H_2L shows characteristics singlet assignable to phenolic (-OH) and aldimine (–CH = N) protons around δ 11.13 ppm and 8.94 ppm, respectively. The presence of base peak at m/z, 397.8 in the HRMS of probe corresponds to $[H_2L+H]^+$. The FT-IR spectrum of H_2L shows a broad band at around 3562.5 cm^{-1} due to phenolic – OH group, whereas the band at 1566.9 cm^{-1} refers to the -C = N (for azomethine) stretching frequency.

The single-crystal X-ray diffraction study allows to establish the detailed structure of H_2L and is comparable with the report[50] in a different form which could be useful for comparison to the current structural characterization (Table 1). The diffraction study shows two half molecules arranged about a crystalloinversion centre. Two different bond lengths of C = N, 1.279(1) and 1.271 (2) Å are comparable with the reported data[51] and the hydrazine N–N lengths of 1.395(7) and 1.401(9) Å, are also similar with published data.[52] The two centro-symmetric H_2L mononuclear unit is connected through H-bonding interactions (^{d}CH•••O = 2.689Å,^{d}CH•••Br = 3.044Å) with molecular synthon $R^4_4(32)$ to form (4,4) net (Figure 1A). H_2L unit exhibits the supramolecular assemblies e.g. CH•••π (^{d}CH•••π = 2.964-3.054Å) and ^{d}NH•••O = 1.922-1.965Å interactions (Figure 1B) to form

451 **Analytical Science Advances**

Full Article
doi.org/10.1002/ansa.202000165

**Chemistry
Europe**
European Chemical
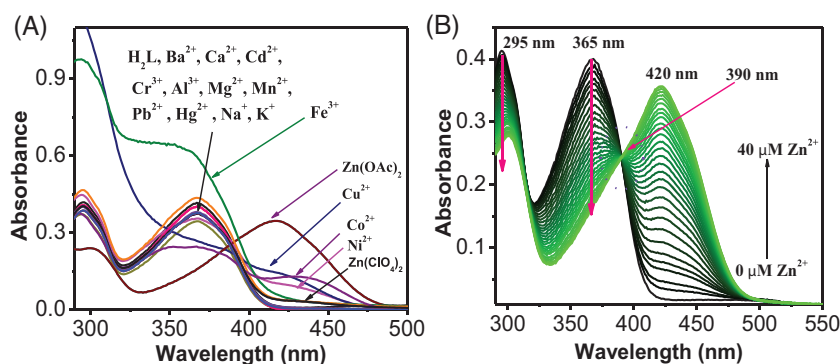Societies Publishing

FIGURE 2 Absorption spectral changes of H_2L (20 µM) upon (A) addition of different cations (B) successive addition of $Zn(OAc)_2$ in DMSO-H_2O (9:1, v/v, 5 µM HEPES buffer pH 7.2)

2D framework (Figure 1C) in crystallographic ac plane to enhance the structural stability of the probe. The two H_2L molecules are arranged in a herringbone fashion when seen down "c" axis (Figure 1D).

3.3 │ Photophysical (absorbance and fluorescence) investigations with metal ions

The absorption and fluorescence behavior of H_2L were studied in DMSO-H_2O (9:1, v/v, 5 µM HEPES buffer pH 7.2). In its absorption spectrum, H_2L (20 µM) exhibits two characteristic peaks centered at 295 nm and 365 nm originating from π-π^* and n-π^* transitions, respectively. To explore the potential use of H_2L as a chemosensor, the absorbance and fluorescence properties of H_2L were compared with before and after addition of 25 equiv. of the alkali metal ions, alkaline-earth metal ions, representative and transition-metal ions (viz., Ba^{2+}, Mg^{2+}, Ca^{2+}, Mn^{2+}, Al^{3+}, Co^{2+}, Ni^{2+}, Cu^{2+}, Cd^{2+}, Pb^{2+}, Hg^{2+}, Na^+, K^+, and Zn^{2+} as their perchlorate salt; Fe^{3+}, Cr^{3+} as chloride salt and also zinc acetate salts, separately. Out of the sixteen metal ions mentioned above, significant absorption spectral change of H_2L was observed with few metal ions like Zn^{2+}, Cu^{2+}, Fe^{3+}, Co^{2+} and Ni^{2+} (Figure 2A). Such type of spectral shift indicates primarily moderate to strong interaction of the probe H_2L toward Zn^{2+}, Cu^{2+}, Co^{2+}, and Ni^{2+} ions. In presence of Cu^{2+}, the UV-spectrum character changes unlikely as compared to other metal ions. Although the copper-mediated hydrolysis of the imine bond is a common phenomenon in presence of water as reported earlier,[53] in our case, it is not due to hydrolysis. Further experiment has been performed to check whether the change in absorption is due to hydrolysis or complexation in presence of Cu^{2+} ion. As depicted in Figure S6, the characteristic peak at 365 nm of the probe H_2L has been restored upon the addition of chelating ligand EDTA to the H_2L-Cu^{2+} ensemble making the probe free and hence we observe the absorption spectrum of H_2L. This confirms that the probe H_2L was not hydrolyzed in presence of Cu^{2+}. While upon addition of Fe^{3+}, it also displays a new absorption band appeared around 450 nm (its own absorption property), and the solution color became yellow. These intriguing absorption signatures of H_2L in the presence of Co^{2+}, Ni^{2+}

and Zn^{2+} is attributed to the ligand to metal charge transfer (LMCT) after formation of individual metal–ligand complexes.

Interestingly, under UV light exposure (366 nm), only the Zn^{2+} added H_2L solution displayed a bright greenish-yellow fluorescence out of the 16 mentioned cations. With the sequential increase of $Zn(OAc)_2$ concentration from 0 µM up to 40 µM, there was a subsequent change of the actual absorption peak at 295 nm and 365 nm with synergic appearances of a new red-shifted (55 nm) band around 420 nm (Figure 2B). The well-defined formation of isosbestic point at 390 nm (Figure 2B) strongly supports the formation of a new complex of H_2L with Zn^{2+}.

Likewise, in the UV-Visible spectral examination, the selectivity of the probe H_2L was verified within the sight of the previously mentioned metal ions through fluorescence study. Though first-row transition metal ions such as Co^{2+}, Cu^{2+}, and Ni^{2+} could coordinate with H_2L, as shown by UV–Vis spectra, they did not show any noticeable emission alternations (Figure 3A). In the emission spectrum, H_2L shows a weak broad two shoulder emission band near 513 nm upon excitation at 410 nm in a DMSO- H_2O (9:1, v/v, 5 µM HEPES buffer pH 7.2). The addition of Cd^{2+} or Mg^{2+} shows very little emission. (Figure 3B). In contrast, the addition of Zn^{2+} affords a very high-intensity emission in the middle region of the spectrum centering at 532 nm. Interestingly and also surprisingly it has been observed that in presence of particular anion (i.e. OAćr) the emission intensity of H_2L-Zn^{2+} ensemble increases tremendously, and also with SO_4^{2-} but not much as that of OAćr (Figure 3C). Furthermore, acetate salt of mentioned metal ion or different metal salt in presence of acetate ion fails to enhance emission intensity to a larger extent as $Zn(OAc)_2$ or Zn^{2+} (as perchlorate) in presence of OAc^- does (Figure S7). Moreover, we have examined the emission response of H_2L with zinc formate and zinc oxalate to demonstrate whether acetate or other carboxylate have any role to augment fluorescence. As depicted in Figure S8, it is observed that the formate and oxalate salts of zinc have a negligible effect to increase emission intensity in comparision to acetate salt of zinc. A gradual increment in the concentration of $Zn(OAc)_2$ to H_2L, a systematic growth in the emission intensity with a 19 nm red-shifted emission maxima was observed (Figure 3D). The color of the solution changed from colorless to green
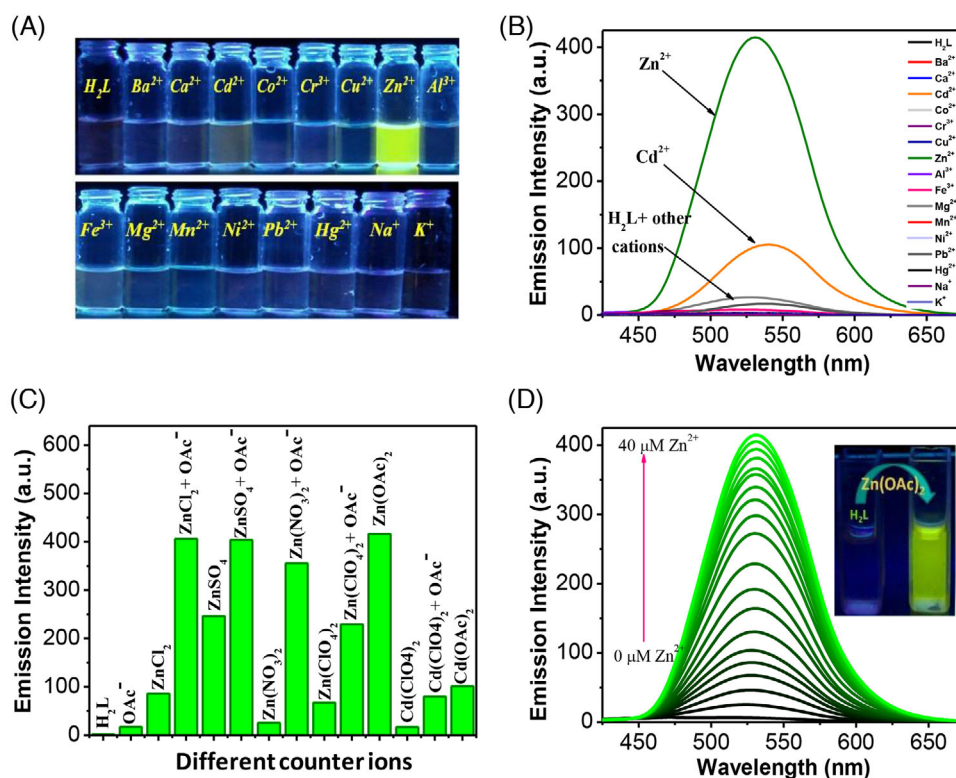
452 | **Analytical Science Advances**

Full Article
doi.org/10.1002/ansa.202000165

**Chemistry
Europe**
European Chemical
Societies Publishing

FIGURE 3 A, Image of H_2L with different cations under UV-lamp. **B**, Emission signature of H_2L with different cations. **C**, Effect of different counter anions on the emission intensity of the H_2L-Zn^{2+} system. **D**, Emission profile of H_2L (20 µM) upon incremental addition of Zn^{2+} in DMSO- H_2O (9:1, v/v, 5 µM HEPES buffer pH 7.2), inset: color change upon the addition of $Zn(OAc)_2$ to H_2L under UV-lamp ($\lambda = 366$ nm). (λex = 410 nm)

during the titration process (Figure 3D, inset). It can likewise be noticed that the fluorescence quantum yield of H_2L ($\varphi = 0.03$) expanded considerably upon cooperation with Zn^{2+} ($\varphi = 0.20$), Cd^{2+} ($\varphi = 0.089$) as their acetate salts. Again, solvent environment plays an important contribution to ion/ molecule sensing. The H_2L binds and sense Zn^{2+} fluorimetrically to the maximum extent in polar aprotic solvents, DMF, and DMSO (Figure S9, S10). Since water content makes an experiment ecofriendly towards real sample analysis, we choose DMSO-H_2O as the medium (9:1, v/v, 5 µM HEPES buffer, pH 7.2) for our present investigation.

3.4 | TCSPC study

Fluorescence lifetime measurements of the H_2L, and related compound have been done in DMSO-H_2O (9:1) at $\lambda_{ex} = 375$ nm. The decay behavior of H_2L and its metal complex were well-fitted to biexponential functions. Bare H_2L showed two components having lifetimes 0.04 (populations 0.99%) and 2.75 ns (populations 0.003%), respectively. The average lifetime of H_2L was calculated to be 0.504 ns. After the addition of $Zn(ClO_4)_2$ solution, lifetime of H_2L changes to 0.25 ns and 1.44 ns, having populations of 0.40 and 0.60%, respectively (Figure 4A). The average lifetime was calculated to be 1.31 ns (Table 2).

The OAc^- salts of other metal ions increase the average lifetime of H_2L from 0.504 ns to 1.00 ns. As appeared in Figure 4B, upon addition of NaOAc followed by $Zn(ClO_4)_2$, the average lifetime was calculated to be 1.53 ns. The direct inclusion of $Zn(OAc)_2$ to H_2L increases the life time to 2.36 ns (Figure 4C). Therefore, the average lifetime of the H_2L increases extremely when both Zn^{2+} and OAc^- ions are present. Hence, OAc^- triggers up the sensing of Zn^{2+} of H_2L. This is attributed to the formation of comparatively rigid structure imposed on the H_2L by strong complexation with Zn^{2+} ion via acetate bridging (Scheme 2). Rigid structural architecture of H_2L inside the complex limits the free movement of flexible bonds and thereby minimizes the radiationless transition and consequently, excited-state lifetime increases.

3.5 | Cross selectivity and sensitivity study

To assess the usefulness of H_2L as a powerful ion-selective fluorescence chemosensor for Zn^{2+}, the impact of competing metal ions is investigated by taking in excess concentration (10 equivalents) of different metal ions as that of Zn^{2+}. The outcome demonstrates that the emission signature of H_2L-Zn^{2+} (as its acetate salt) solution remains unchanged by the presence of common cations except by Cu^{2+}, Fe^{3+},
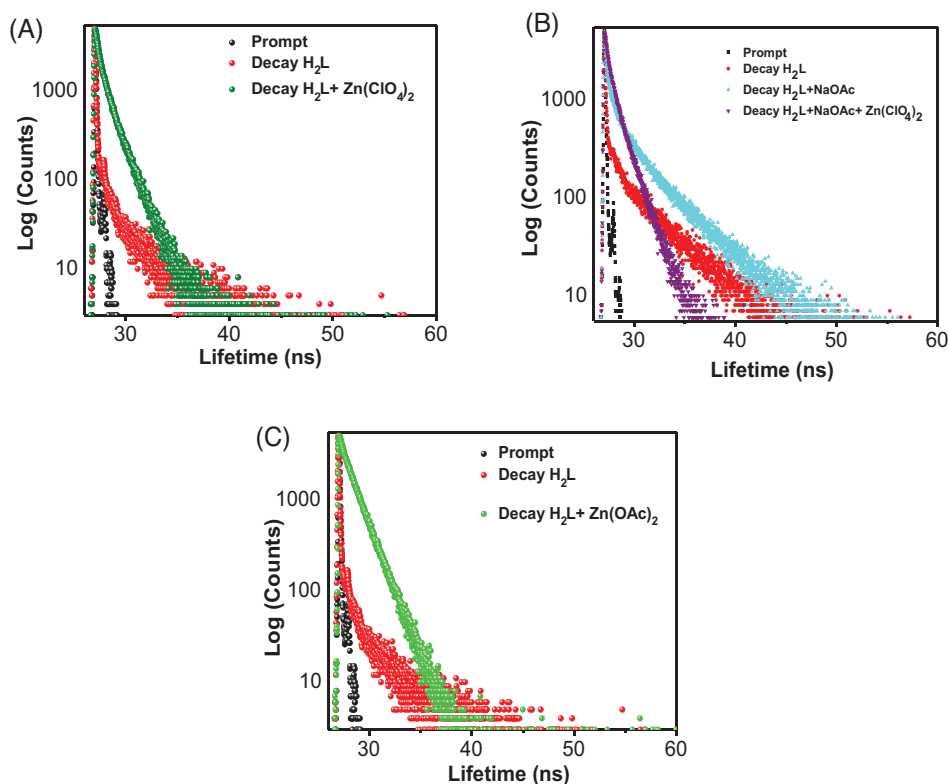
FIGURE 4 Time-resolved fluorescence decay graph of **A**, H_2L (red), H_2L+$Zn(ClO_4)_2$ (dark green), **B**, H_2L (red), H_2L + NaOAc (cyan), H_2L + NaOAc + $Zn(ClO_4)_2$ (purple), and **C**, H_2L (red), H_2L+$Zn(OAc)_2$ (bright green) in DMSO-H_2O (9:1) at 298 K (λex = 375 nm)

TABLE 2 Fluorescence lifetimes of H_2L and H_2L - complex in DMSO-H_2O solvent

DMSO-H_2O (9:1)	τ_1 (ns)	τ_2 (ns)	α_1	α_2	χ^2	τ_{av}
H_2L	0.04	2.75	0.997	0.003	1.07	0.504
H_2L + $Zn(ClO_4)_2$	0.25	1.44	0.40	0.60	1.02	1.31
H_2L + NaOAc	0.29	1.37	0.71	0.29	1.04	1.001
H_2L + NaOAc+ $Zn(ClO_4)_2$	0.06	3.82	0.99	0.01	1.06	1.53
H_2L + $Zn(OAc)_2$	0.24	3.53	0.89	0.11	1.11	2.36

Co^{2+}, and Cr^{3+}. These four cations quench the emission intensity to a large extent (Figure 5A) due to their strong complexation tendency which replaces the Zn^{2+} from the formed complex, heavy atom effect and paramagnetic quenching efficiency.[54–56]
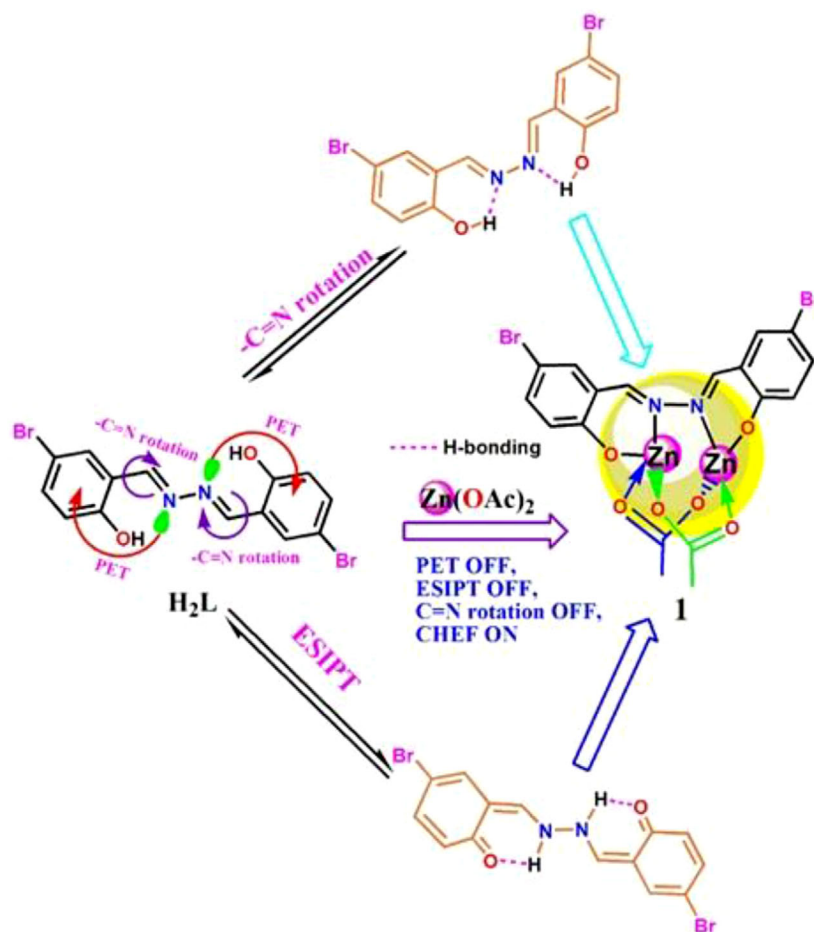
The possible disruption of anions was also investigated by the competitive experiments with excess (10 equivalent) of anions in a similar manner. The emission profile of H_2L-Zn^{2+} (in its acetate salt) solution remains almost unaffected by the presence of common anions such as F^-, Cl^-, Br^-, I^-, OAcŕ, NO_2^-, NO_3^-, PO_4^{3-}, S^{2-}, $S_2O_3^{2-}$, SO_4^{2-}, SO_3^{2-}, HSO_3^-. However, HSO_4^-, HPO_4^{2-} and $H_2PO_4^-$ quenches the intensity to a noticeable extent (Figure 5B) as seen in some literature.[57–59] These all outcome suggesting that the probe H_2L is an AcO$^-$ specific fluorescence chemosensor for Zn^{2+} even in the presence of most of the competing ions (cations and anions).

3.6 | Reversibility

To investigate the reversibility of the sensor toward Zn^{2+}, strong chelating agent EDTA was added to the sensor H_2L-Zn^{2+} complex, and the absorbance, as well as fluorescence response, was noted (Figure S11a, 11b). With the addition of 1.0 equivalent EDTA as that of Zn^{2+} to the sensor H_2L-Zn^{2+} complex, the absorbance of the receptor recovered. Again, the greenish fluorescence is fully quenched on the addition of EDTA to the H_2L-Zn^{2+} ensembles and this indicates the metal ion is completely stripped away from the complex to make the ligand bare again. Further inclusion of Zn^{2+}, the emission intensity was recovered. The fluorescence emission changes show a twisting response even after several cycles (Figure S12) and the sensor can be easily recovered for repeated use.

3.7 | pH effect on sensing behavior

The fluorescence intensity of the H_2L is very low or negligible and didn't differ remarkably over a wide pH range from 2.0 to 8.0 (Figure 6). Beyond pH 8.0, the fluorescence intensity turned out to be high. At lower pH the imine protons get protonated or the compound may get hydrolyzed to discharges non-fluorescent beginning aldehyde. While in the moderate range of pH the ESIPT process (discussed later) prevails to show the two shoulders in its emission spectra. In the span

454 | **Analytical Science Advances**

Full Article
doi.org/10.1002/ansa.202000165

Chemistry Europe
European Chemical
Societies Publishing

SCHEME 2 Plausible binding and sensing mode of the chemosensor H_2L towards Zn^{2+}

of higher pH (>10), deprotonation of hydroxyl group takes place and consequently able to dismiss the ESIPT procedure, thus results in high emission. Again, the emission profile of H_2L-Zn^{2+} complex displayed remarkably higher intensity between the pH ranges from 6.5 to 9.5. Henceforth, the probe can be useful for Zn^{2+}-sensing under physiological pH ranges.

3.8 | Detection limit and binding stoicheometry

From the emission titration, detection limit (LOD) for Zn^{2+} is determined to be 2.18 µM using 3σ method (Figure S13), which is far better than the acceptable limit of 76 µM Zn^{2+} recommended by the US-EPA and World Health Organization (WHO) for drinking water.[60] Moreover, to determine the stoichiometry of the H_2L/Zn^{2+} complex further, Job's method using fluorescence intensity was applied to keep the total concentration of Zn^{2+} and H_2L at 10 µM, but changing the molar ratio of Zn^{2+} from 0 to 0.9. A plot of fluorescence intensity at 532 nm versus X_M shows that the value goes through a maximum at a molar fraction of about 0.69 (Figure S14), indicating a 1:2 stoichiometric complex formation exactly. Again, the plot of $\{(F_{max} - F_0)/(F - F_0)\}$ vs. $1/[Zn^{2+}]^2$ yields a straight line (Figure S15), indicating that H_2L binds with Zn^{2+} in a 1: 2 stoichiometry with association constant (ka) = 1.2×10^{10} M^{-2}

determined from Benesi-Hildebrand equation. This illation was further ascertained from the ESI-MS spectrum (Figure S16), which exhibited peaks at m/z = 645.43 corresponding to 1: 2 $[L^{2-} + 2Zn^{2+} + 2OAc\acute{r}]$ complexation.

3.9 | Plausible binding mode eluciation

In order to verify the binding site of ligand metal complex, ^1H NMR titration were performed using 0 and 2.0 equivalent Zn^{2+} ion in DMSO-d_6 (Figure S17). The bare ligand H_2L showed characteristic –O-$\underline{H}$ peak at 11.13 ppm, –$C\underline{H}$ = N- peak at 8.94 ppm and other remaining aromatic protons at desired position. When, $Zn(ClO_4)_2$ was added to probe the peaks corresponding to –O-H disappeared indicates the probe binds the metal ion through deprotonated hydroxyl group as shown in Scheme 2. FTIR of H_2L shows -OH stretching frequencies 3562.5 (hydrogen bonded, broad, Figure S5). Formation of the L–Zn^{2+} complex shifts the –OH stretching frequency from 3562.5 cm^{-1} to a broader value in the region 2955 cm^{-1} indicates the co-ordination occurred hydroxyl oxygen atom since on binding to the metal center the electron density on the donating center decreases and hence made the related bonds weaker than before binding. The stretching band appeared at 1625 cm^{-1} assign to be –C = N- bond in free H_2L shifted to 1600 cm^{-1}
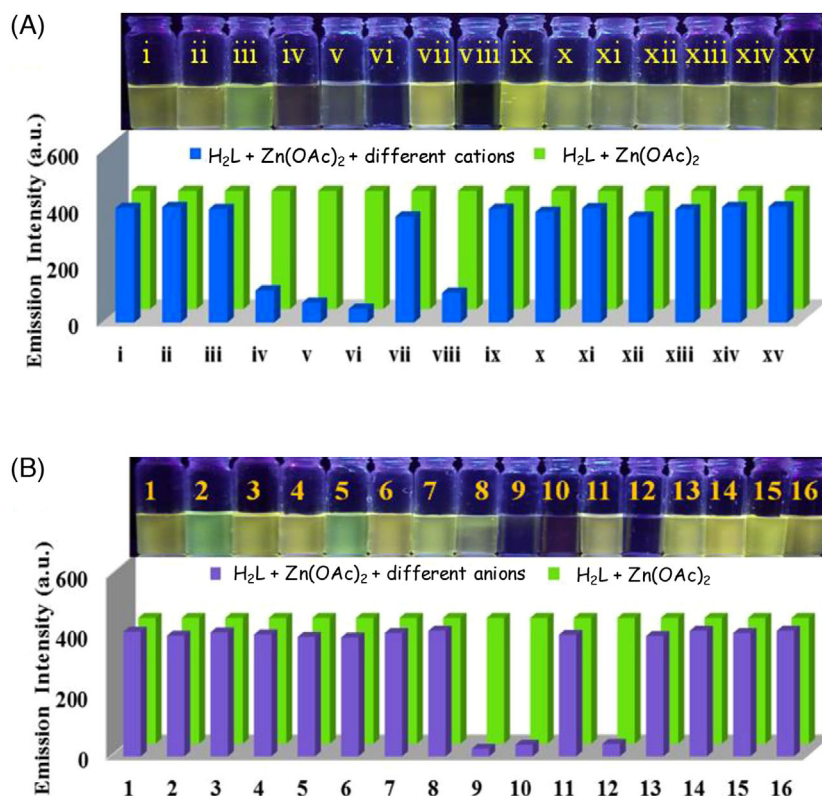
455   **Analytical Science Advances**   Full Article
doi.org/10.1002/ansa.202000165

Chemistry
Europe
European Chemical
Societies Publishing

FIGURE 5   **A**, Competing cations effect on emission intensity of H_2L-Zn^{2+} complex, inset: corresponding image under UV cabinet (366 nm) [i. Ba^{2+}, ii.Ca^{2+}, iii.Cd^{2+}, iv.Co^{2+}, v.Cr^{3+}, vi.Cu^{2+}, vii.Al^{3+}, viii.Fe^{3+}, ix.Mg^{2+}, x.Mn^{2+}, xi.Ni^{2+}, xii.Hg^{2+}, xiii.Pb^{2+}, xiv.Na^+, xv.K^+). **B**, Competing anions effect on PL intensity of H_2L-Zn^{2+} complex, inset: corresponding image under UV cabinet (366 nm)[1. F^-, 2.Cl^-, 3.Br^-, 4.I^-, 5.OAc^-, 6.NO_2^-, 7.NO_3^-, 8.PO_4^{3-}, 9. HPO_4^{2-}, 10$H_2PO_4^-$, 11.S^{2-}, 12.HSO_4^-, 13.$S_2O_3^{2-}$, 14.SO_4^{2-}, 15.SO_3^{2-}, 16.HSO_3^-]

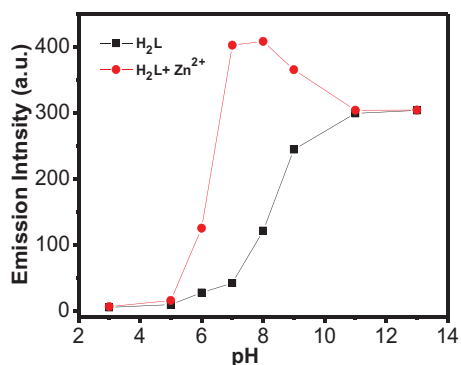**FIGURE 6**   pH change effect on emission behavior for H_2L and H_2L -Zn^{2+}

in complex lowered the bond strength by decreasing the electron density on aldimine N-atom in complex (Figure S18).

3.10 | Microscopic studies

Comparative analysis of the SEM images of H_2L in the absence and presence of Zn^{2+} ions shows major morphological variations, as shown in Figure 7. The probe H_2L exhibits a rod-like structure in its free state

(Figure 7A). However, in complex molecule, obtained from the ligand with Zn salt, the structure is comparatively smaller (Figure 7B). This is due to the agglomeration of receptor H_2L with Zn^{2+} ions. EDAX analysis (Figure 7C) indicates the presence of carbon (C), oxygen (O), nitrogen (N) and bromine (Br) in receptor H_2L in atomic percentages are 70.42, 10.74, 9.13, and 9.70, respectively. EDAX analysis of H_2L–Zn^{2+} (Figure 7D) gives the result having atomic percentage carbon (C), oxygen (O), nitrogen (N), bromine (Br), and zinc (Zn) 57.71, 6.28, 22.81, 4.22, and 8.98, respectively. This outcome further confirms the complex formation with 1:2 stoichiometry.

3.11 | Plausible sensing mechanism

In the absence of a metal ion, H_2L did not show noticeable intense emission when excited at 410 nm because the cis- trans isomerization around -C = N- bond may be the predominant decay process in the excited state.[61] This was confirmed from the viscosity dependent emission of the probe as shown in Figure 8. With increase of viscous solvent glycerine in DMSO-glycerine mixture the emission intensity emerged. This supports free rotation around the –C = N- inhibited resulting in the suppression of the non radiative decay process in the excited-state. When the probe binds Zn^{2+} associated with acetate ion (shown in Scheme 2) such type of isomerization process
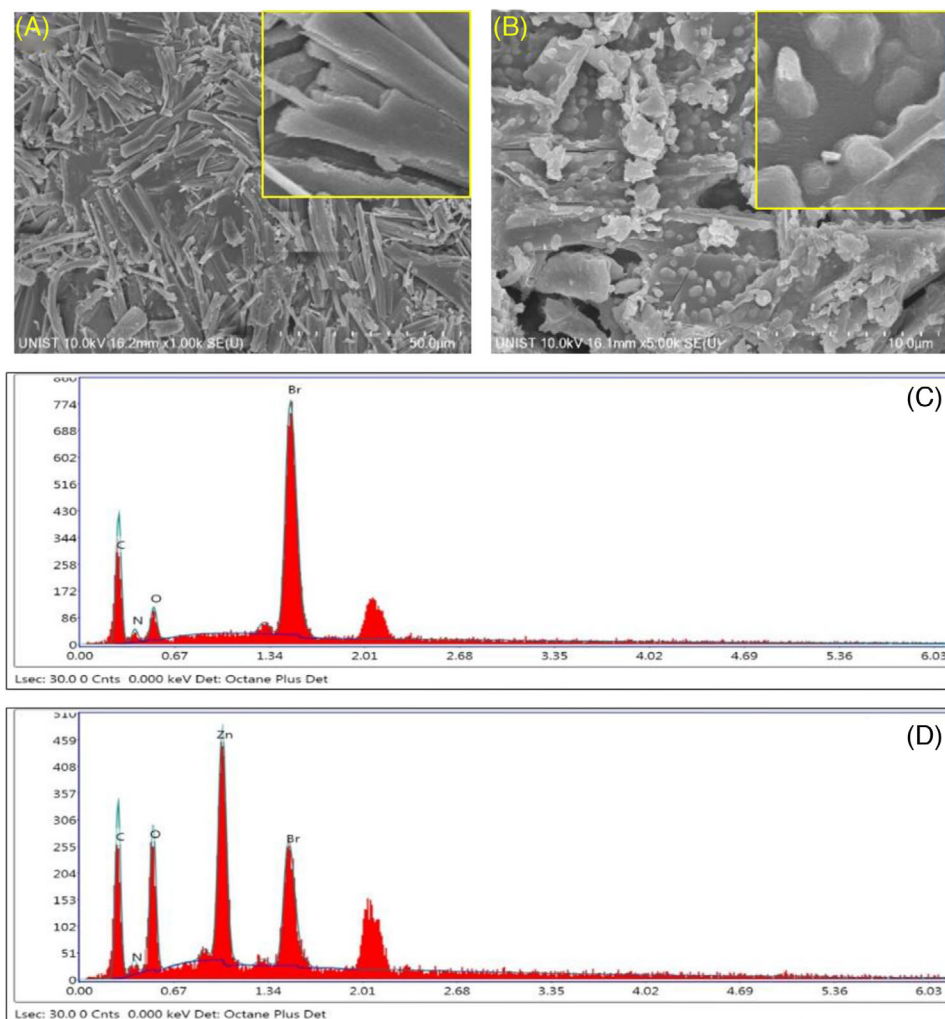
456 | **Analytical Science Advances**

Full Article
doi.org/10.1002/ansa.202000165

Chemistry Europe
European Chemical
Societies Publishing

FIGURE 7 SEM images of (A) Receptor H_2L (inset: zoom view). (B) Receptor H_2L-Zn^{2+} (inset: zoom view), (C) EDAX analysis report of receptor H_2L. (D) EDAX analysis report of receptor H_2L-Zn^{2+} complex
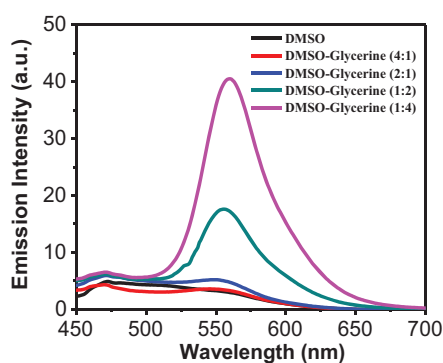

FIGURE 8 Viscosity dependent emission profile of the probe H_2L (20 µM) in different DMSO-glycerine content content (λ_{ex} = 410 nm)

completely locked and hence the strong emission takes place from the system.

From the emission titration plot, it was easily noticed that although there was a huge emission intensity increases when Zn^{2+} added to the receptor, only a small spectral shift (19 nm, from 512 nm to 531 nm) occurred with this receptor. This observation proposed PET on-off mechanism since PET sensors usually exhibit increase or decrease in emission intensity but show little or no spectra shift.[15,62] In presence of Zn^{2+}, aldimine N-atom gets involved in co-ordination with metal ions inhibits the PET process which was again confirmed from FTIR spectra.

From the viewpoint of ESIPT, nearness of acidic salicyl—OH and basic imine-N moieties favorable for six-membered ring structure via intramolecular H-bonding is of special interest.[63] Upon excitation, the proton is transferred from the hydroxyl oxygen to the electronegative imine nitrogen of the internal hydrogen-bonded enol isomer framing an excited state K*, which happens extremely fast in the sub-picosecond time scale.[64] After the relaxation of the keto form (K*) to the ground state, the energetically favored enol form is recuperated spontaneously by reverse proton transfer, to finish the cyclic four-level scheme.[65] Again, the intramolecular hydrogen bonding (-OH···N-) needed for the ESIPT process is interrupted in polar protic solvent via intermolecular H-bonding. Whereas, in polar aprotic

TABLE 3 solvent effect on absorbance and fluorescence spectra of the probe H_2L

Solvent	Abs. max	Em. Max	Polarity index	Stokes shift
MeOH	293, 365	468, 542	5.1	175, 177
MeCN	294, 368	471, 533	5.8	177, 165
DMSO	294, 367	470, 529	7.2	176, 162
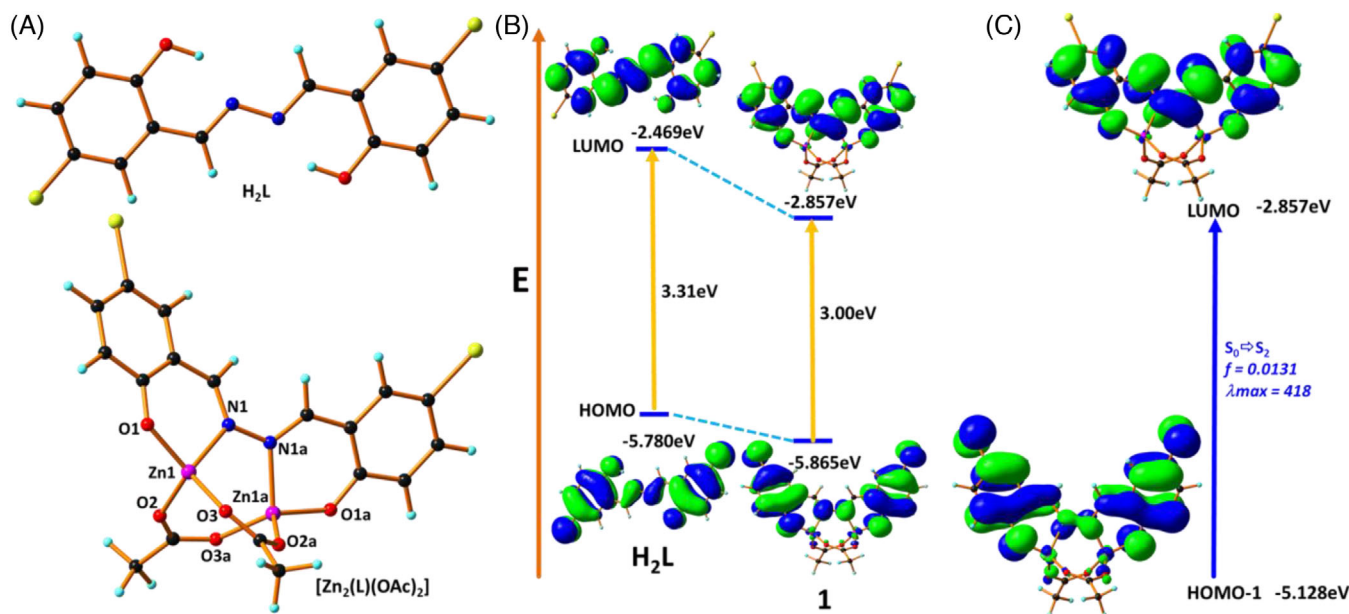
FIGURE 9 A, Geometry optimized molecular structures of H_2L and $[Zn_2(L)(OAc)_2](1)$; a = symmetry related; B, comparable HOMO-LUMO energy difference for H_2L and **1**; C, frontline molecular orbitals elaborate in the absorbance of **1** in DMSO solution

solvent intermolecular H-bonding also possible but it occurred only with phenolic H-atom, imine N-atom unable to form H-bond as in methanol.[66] To confirm the phenomenon of photo-tautomerism, we have explored the solvents effects on photophysical behavior of the probe H_2L and its Zn^{2+} -complex in terms of absorbance and emission study. We have chosen MeCN and DMSO as polar aprotic and MeOH as polar protic solvents in this context. The UV-Vis absorption peaks centered at 293 nm in MeOH, 294 nm in DMSO and 293 nm in MeCN can be attributed to π-π^* transition. The longer absorbance peak at 365 nm in MeOH, 367 nm in DMSO and 368 nm in MeCN can be attributed to n- π^* transition. The absorbance peaks of H_2L appeared almost in the same position, demonstrating a comparable ground-state type in all solvents. The slightly blue-shifted in methanol is not consistent with simple polarity effects and may be due to specific H-bonding interaction with methanol donor and the imine nitrogen acceptor. The corresponding emission peaks were observed at 468 nm, 542 nm in MeOH; 470 nm, 529 nm in DMSO; 471 nm, 533 nm in MeCN, respectively. The Stokes shifts were 177 nm, 162 nm, and 165 nm in MeOH, DMSO, MeCN respectively [Table 3].

The emission wavelength and Stokes' shift decrease with increasing solvent polarity (Figure S6, S7), suggesting in excited-state (K* state) has lower population than E* state. These findings are comparable

to various other ESIPT systems.[66,67] The bi-exponential decay fitting also supports the ESIPT process to take place, one from keto another from enol. The lifetime of the Zn^{2+}-receptor ensembles increases from 0.504 ns in free probe to 2.36 ns and this strongly supports the inhibition of the ESIPT process on complex formation. Again, highest lifetime for Zn-acetate associated receptor confirms that acetate ion makes an effective platform for Zn^{2+} sensing. These collective experimental results like [1]NMR, IR, UV-Vis absorbance, fluoresccence (both steady-state and time-resolved), ESI-MS and SEM indicate Zn-acetate or Zn^{2+} ion in the presence of acetate ion capable to lock the free rotation around –C = N bond completely, restrict ESIPT and PET process leading to sense fluorimetrically.

3.12 | Geometry optimization studies

To validate the interaction of the probe H_2L and Zn^{2+}-L complex, we have performed density functional theory (DFT) utilizing Gaussian 09 software on their geometries. The theoretical geometries of H_2L and its Zn(II) complex are revealed in Figure 9a. The conformation and coordination of the neutral complex as $[Zn_2(L)(OAc)_2](1)$ is confirmed from ESI-MS spectra and then executed the theoretical optimization on it.

458 | **Analytical Science Advances**

Full Article
doi.org/10.1002/ansa.202000165

Chemistry Europe
European Chemical
Societies Publishing

TABLE 4 The comparable calculated absorbance λ_{max} with experimental values for **H₂L** and **1**

Ligand and Complexes	Theoretical (nm)	Experimental (nm)	Composition	Electronic Transition	Energy (eV)	F
H₂L	295 354	295 365	HOMO→LUMO+1 HOMO-2→LUMO	$S_0 \rightarrow S_5$ $S_0 \rightarrow S_3$	4.1905 3.6382	0.0975 0.0726
L-Zn²⁺	413	418	HOMO-1→LUMO	$S_0 \rightarrow S_2$	3.0006	0.0131

The main bond lengths and bond angles of the complex are tabulated in Table S1.

For complex 1, each metal atom Zn^{2+} is being tetra-coordinated with mono-deprotonated (with NO donor sites) of one side of bi-compartmental tetra-dentate **H₂L** ligand and two acetate (OAcŕ), co-ligands bridges to each metal centers to an arrangement of a tetrahedral geometry with inversion center and combined to form a binuclear neutral complex with a frame of $[Zn_2(L)(OAc)_2]$(1). The calculated Zn–N bond distances are span in the range 2.028 Å and Zn–O bond distances are fall in the range 1.906-1.972 Å.

In the case of **H₂L**, the electron cloud remains mainly on HOMO–1, LUMO, and LUMO+2 orbital ensues at the phenoxo oxygen and phenyl ring, while the same for HOMO-3, HOMO, HOMO–2, and LUMO+1 orbitals reside at the phenyl ring and phenoxido oxygen, bromine atoms as well as at azine nitrogens atom with an energy difference between HOMO and LUMO of 3.31 eV (Figure 9B). Just in case of complex 1, HOMO, HOMO–1 and LUMO orbitals mostly originate from the involvement of azine nitrogens, phenyl ring, and phenoxido oxygen, and also LUMO+1, LUMO+2, LUMO+3, and HOMO–2 orbitals originate from azine nitrogens, phenoxido oxygen, and considerable contribution of metal centers with an energy difference between HOMO and LUMO of 3.00 eV (Figure 9B).

The absorbance spectra of the ligand used in the present work were studied at room temperature in DMSO. The ligand shows two well-resolved peaks at 295 nm and 365 nm that are in well agreement with theoretical values at 295.87 nm and 353.79 nm, respectively. These bands are assigned to $S_0 \rightarrow S_5$ and $S_0 \rightarrow S_3$ electronic transitions for **H₂L**.

The complex 1 shows well-consigned absorbance band at 418 nm (Figure 9C) in DMSO solvent at 298K and the corresponding calculated absorption band is located at 413.20 nm which is in excellent agreement with experimental result (**Table 4**). This spectrum band can be assigned to the $S_0 \rightarrow S_3$ transition.

3.13 | Aggregation-induced emission characteristics of the probe H₂L

The nearness of ESIPT and C=N isomerization properties in **H₂L** influence to test its AIE character. The presence of bromine substituent boosts the emission intensity.[28] SCXRD reveals that intermolecular Br⋯Br halogen bonds as well as multiple stronger intermolecular interactions in the crystal may lead to a more rigid environment, which can substantially suppress molecular motions and facilitates the emission process in its aggregate state. The sensor is well soluble in DMF and DMSO yet is insoluble in water. The probe **H₂L** in its absorption spec-
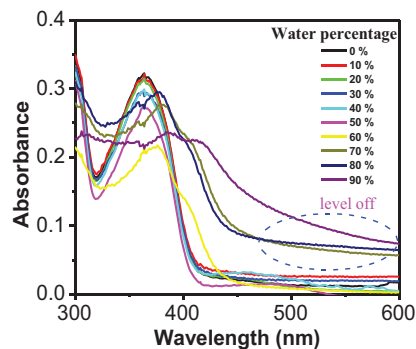
FIGURE 10 Absorption profile of the probe **H₂L** (20 µM) in different DMSO-H₂O ratio

trum shows a longer wavelength level off pattern (due to Mie effect) with more than 60% water content in DMSO-H₂O binary mixture indicating formation of nano aggregate (Figure 10).

The probe **H₂L** in DMSO with increasing water fraction from 0% to 90% shows the solution color changing from a non-emissive to brightly greenish yellow under UV light (366 nm) exposure (Figure 11A). Upon excitation at 410 nm, the sensor **H₂L** is non-emissive and the emission profile of the sensor is nearly unaltered at 0%–40% water fraction at 530 nm (Figure 11B). The fluorescence intensity increases surprisingly at 560 nm when the water fraction becomes ≥ 50%. Beyond the 70% water content in the binary mixture the intensity gets to fall. The different organic solvent and water mixture (3:7) like DMF-H₂O, DMSO-H₂O, MeCN-H₂O. MeOH-H₂O, EtOH-H₂O, THF-H₂O also show the same type of emissive character of **H₂L** (Figure S19). The actual emission color perception for **H₂L**+Zn²⁺ is best viewed by popular CIE 1931 diagram (Commission International de L'Eclairage) by using the co-ordinates CIE-X 0.28 and CIE-Y 0.60 for its emission that dictates its color in green region. The AIE state have the co-ordinates CIE-X 0.42 and CIE-Y 0.51 that indicates the color toward more yellow color (Figure 11C).

The DLS based particle size analysis of **H₂L** (20 µM) in different water fraction roughly give the idea of the aggregation (Figure S20, a-f). With increment water content the molecule gets assembled to a largest aggregate at 50% water fraction with single particle distribution of value 441 nm. Further increase of water fraction (60%) makes the aggregate larger but unequal sized with major distribution of 268 nm particle. At 70% water content, mainly two particles of size 214 nm and 609 nm contribute to nearly 1:3 ratio. Further increase of water fraction makes the particle smaller in size. This indicates aggregation of the probe takes place up to 70% water and after 70% water content the
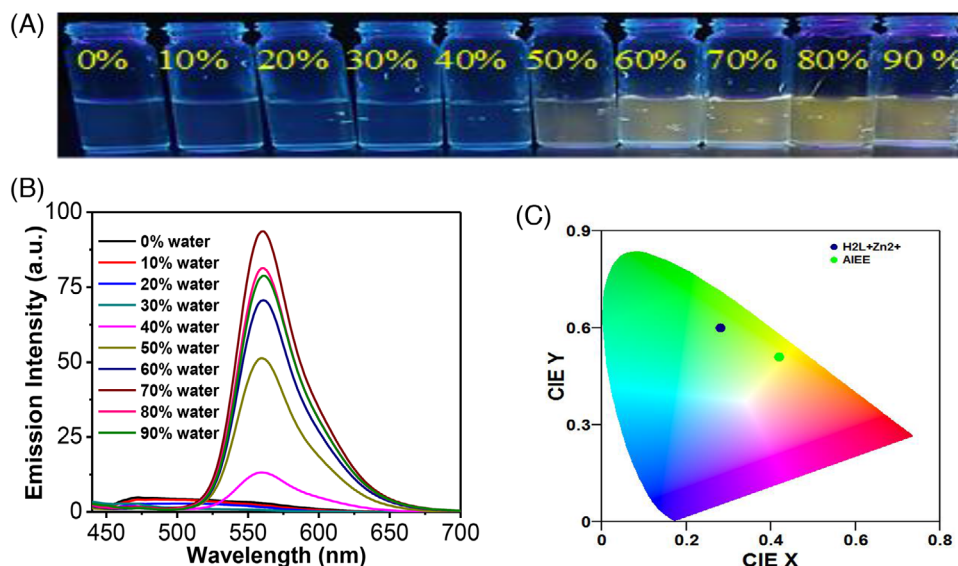
FIGURE 11 **A**, Image of the probe H_2L (20 µM) in different DMSO-H_2O ratio under UV-cabinet (λ = 366 nm) **B**, Emission profile of the probe H_2L (20 µM) in different DMSO-H_2O ratio. (λex = 410 nm, slit width = 2.5 nm/2.5 nm). **C**, Chromaticity diagram from PL spectra of H_2L+Zn^{2+} and H_2L in aggregate state

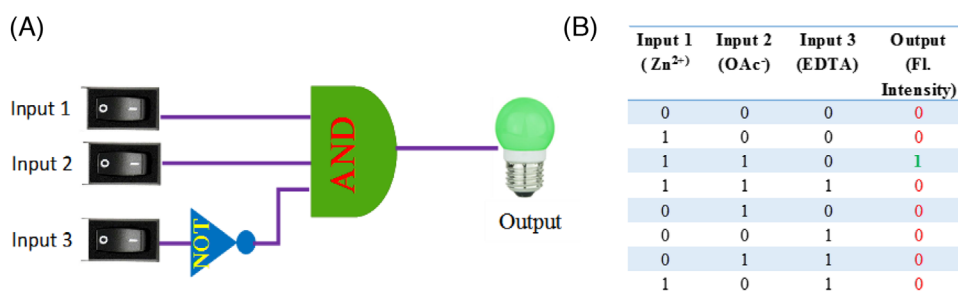**FIGURE 12** **A**, Representative combinational logic gate circuit. **B**, Corresponding truth table

agglomeration begins. This phenomenon demonstrated that the sensor is an AIE-active compound.

3.14 | Molecular logic gate

The variation of the optical outputs with a reasonable mix of different ionic inputs can be utilized to impersonate different Boolean logic operations. The function of the memory device in the current case is based on Boolean logic which switches between two crisp states, either "0" or "1." By utilizing Zn^{2+}, OAcŕ, and EDTA as the three input and ensuing changes of emission intensity on the interaction of H_2L with the mentioned three analytes as output signal, a combinational logic gate can be constructed based on NOT and AND gates.

The three chemical inputs of Zn^{2+}, OAcŕ, and EDTA ions are assigned as input 1, input 2, and input 3, respectively, and considered as logic 1 when they are available and logic 0 stands for no addition of Zn^{2+}, OAcŕ, EDTA. The output corresponds to the turn-off and turn-on fluorescence emission at 532 nm denoted by Logic 0 and Logic 1,

respectively. The three possible input and fluorescence signal as output meet the character of a combined NOT and AND type molecular logic gate as shown in Figure 12A. Under the conceivable eight combinations of these inputs, the condition (110) displays the output as 'ON' with the readout signal '1'. However, the rest of the seven combinations exhibits no change in the fluorescence intensity of H_2L, through displaying the output as 'OFF' with the readout signal as 0 (Figure 12B, table).

3.15 | Molecular memory device

Memory devices are gadgets that are fit for taking care of information and can be created by sequential logic circuits. These circuits function through the feedback loop in which one of the outputs of the device fills in as the input information and it is remembered as a "memory element". So by utilizing binary logic function, a sequential logic circuit has been designed displaying "Write-Read-Erase-Read" kind of behavior.

In our system, high emission output at 532 nm and weak emission output at the same wave-length have been considedered as ON
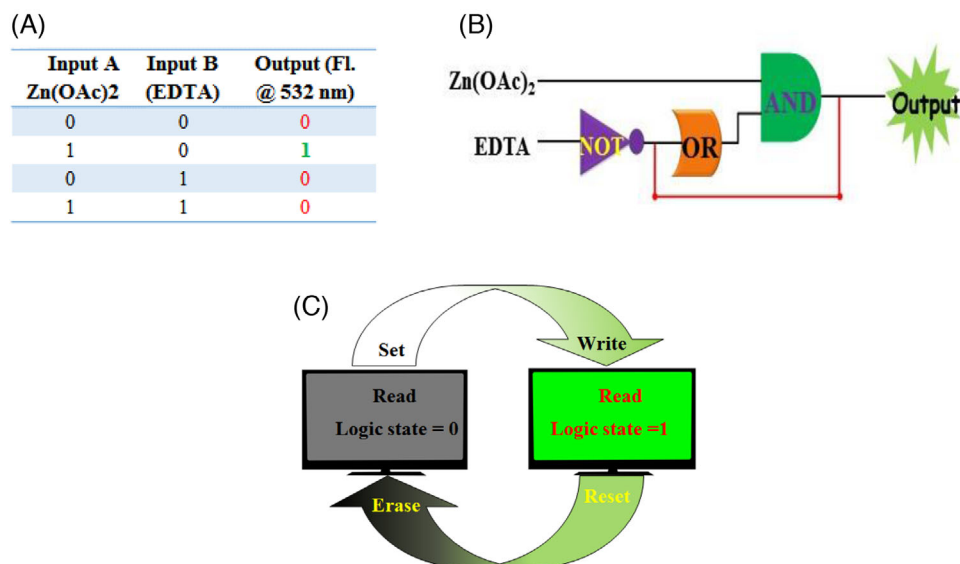
FIGURE 13   A, Truth table of the logic circuit. **B**, Schematic circuit diagram of logic gate for molecular memory device; **C**, Schematic representation for the memory element with "writing-reading-erasing-reading" property

TABLE 5   Brief comparison between recently published works based on synergistic sensing with our probe H_2L

Sl. No.	Probe	Analytes	Detection limit	Mechanism	Reference
1	Probe 1	Zn^{2+}, F^-	LOD not given	ESIPT	[68]
2	Probe 2	Mg^{2+}, Na^+	LOD not given	ICT	[69]
3	Probe 3	Zn^{2+} and Pb^{2+} via Au^+	LOD not given	AIE	[70]
4	Probe 4	Cu^{2+} ions via Zn^{2+} or Cd^{2+}	5.07×10^{-8} M for Zn^{2+} and 4.68×10^{-8} M for Cd^{2+},	PET	[71]
5	Probe 5	Zn^{2+}, OAcŕ	2.4×10^{-7} M for Zn^{2+}	ESIPT	[72]
6	**Probe H_2L**	**Zn^{2+}, OAcŕ**	**2.18×10^{-6} M for Zn^{2+}**	**PET, CHEF, C = N isomerization, ESIPT, AIE**	**This work**

state (1) as OFF state (0), respectively. Now for the construction of useful mimic of memory element of our receptor H_2L, we took $Zn(OAc)_2$ and EDTA as the inputs for the Set (S) and Reset (R) process, respectively and emission intensity at 532 nm is considered as the output signal (Figure 13A,B). In this memory function, the system writes when it gets input A (Zn-acetate) i.e. high emission value and it memorizes binary number "1" that results in writing 1. But the input B (EDTA), which is a reset input, erases the data resulting in writing and then memorize the binary number 0 (Figure 13C). The most noteworthy thing is that these cycles could be repeated many times (Figure S12) with the same concentration of the input without a remarkable decrease in emission intensity. Thus, this molecular sequential logic function based circuits shows near sort of behavior like the traditional semiconductor based logic devices, and it may be a well tool for improvement of molecular microprocessor in near future.

The novelty of our as-synthesized probe on the basis of synergistic sensing shown in the Table 5 presents that H_2L is an outstanding performer as a chemosensor of Zn^{2+} and OAcŕ.

3.16 | Application of probe H_2L-aggregate as a picric acid (PA) sensor

The photoluminescence property of the probe in solid-state as well as with a higher percentage of water inspired us to check or develop it as a picric acid sensor, for this goal we used 70% water content of H_2L (20 µM) solution in acetonitrile and various nitro-aromatics was added. The selectivity and sensitivity of the probe were investigated using various analytes (150 µM) such as nitrobenzene (NB), 2- aminophenol (2-AP), 2-nitrotoluene (2-NT), p-nitrobenzoic acid (4-NBA), 1,3- dinitrobenzene (DNB), o-nitrophenol (2-NP), 3-nitrophenol (3-NP), 4-nitrophenol (4-NP), 2,4-dinitrophenol (DNP), and picric acid/trinitrophenol (PA/TNP) by means of emission changes . The emission spectra show that only PA and 2,4-DNP quench the luminescence properties of which former quenches a large extent (Figure 14A). Successive addition of PA decreases the emission intensity at 560 nm gradually (Figure 14B).

It is fascinating to note that among various investigated nitroaromatics, only PA cause to be significant fluorescence turn-off responses,
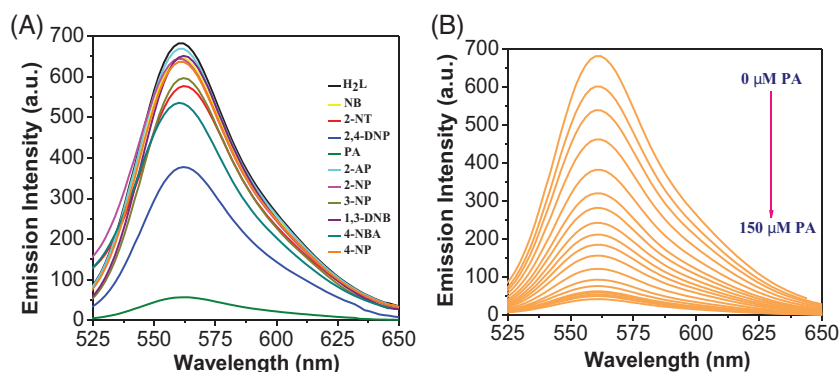
FIGURE 14 A, Fluorescence spectra of H_2L (20 μM) in the presence of various NAC's in DMSO-H_2O (3:7) (Excitation at 410 nm, Slit width = 5 nm /5nm). B, Fluorescence responses of H_2L (20 μM) toward different concentrations of PA in aqueous (0-150 μM) solution

which undoubtedly indicates that strong ground state complexation between highly electron deficient PA and more electron-rich fluorescent hydrosol causes fluorescence quenching more easily via charge transfer pathway. Again, as the absorption band of PA falls (365 nm) within the area of absorption maxima of aggregated H_2L, the quenching in emission intensities on excitation at higher wavelength (410 nm) eliminated the scope of inner filter effect (Figure S21). Again, the optimized DFT calculation shows energy of HOMO and LUMO of picric acid is far below the HOMO and LUMO of the probe H_2L (Figure S22). Therfore the charge transfer mechanism is responsible for PL quenching phenomenon. Due to the presence of three strong electron-accepting group in PA, it is an effective molecule over other nitroaromatics for reducing the emission intensity. In solution, the quenching was observed under UV- light (366 nm) (Figure S23a). Furthermore, to develop an inexpensive and convenient tool for PA detection, test strips were prepared from Whatman 41 filter paper using probe H_2L solution (20 μM). The test strips were spotted by solution of H_2L and then dried in air. The probe H_2L-immersed filter paper strip showed an intense yellowish fluorescence on exposure to UV-light. Insignificant quenching of yellowish emission intensity upon the addition of different analytes (50 μM) was observed except PA and 2,4-DNP quench to marked extent (Figure S23b). Furthermore, PA solutions of different concentrations (10^{-2} –10^{-7} M) were prepared and 0.02 mL of each was dropped on each fresh test strips (Figure S23c). Visual color changes were noticed from colorless to yellow in the case of 10^{-3} M concentration while on the addition of further diluted concentration, no color change was observed. Under the UV light (366 nm), detectable dark spot was observed in the case of 10^{-3} M concentration which faded upon further dilution. Thus, paper strips application pave a cheap onsite kit for picric acid detection.

4 | CONCLUSIONS

We have successfully synthesized and characterized a salen-based inexpensive turn-on fluorescent probe for the selective determination of Zn^{2+} in presence of OAcŕ ion. Zn^{2+} produces a pronounced

fluorescence enhancement response under an OAcŕ triggered synergistic effect which is reported for the first time in the current study. Our as-synthesized probe offers selective Zn^{2+} detection in the presence of several other metal ions up to micromolar limits. Fluorescence enhancement is attributed to the Zn^{2+} assisted CHEF process, and inhibition of PET and ESIPT process. The binding mode was well corroborated with the theoretical study. Based on the three chemical inputs of Zn^{2+}, OAcŕ, and EDTA ions, and emission intensity as output advanced level molecular logic gates including memory device is possible with suitable selection of inputs. Our fundamental findings will pave the way for design and synthesis of counter anion triggered chemosensors which will also be highly beneficial as solid-state emitter. Moreover, the application for picric acid detection using the AIE probe is also promising.

CONFLICT OF INTEREST

The authors declare no conflict of interest.

ORCID

Bhriguram Das https://orcid.org/0000-0001-8938-0123

REFERENCES

1. Frio A, Janeiro R, De; Viana SM, Valladares CS, Duarte BP. *Geoquímica dos ortognaisses do Complexo Região dos Lagos,. Front. Issues Econ. Thought.* Washington, D.C: Isl. Press; 2001:6.
2. Emas R. The concept of sustainable development : definition and defining principles. *Br GSDR.* 2015:1-3.
3. Brodowska K, Łodyga-Chruścińska E. Schiff bases - Interesting range of applications in various fields of science. *Chemik.* 2014;68:129-134.

4. Kumar S, Dhar DN, Saxena PN. Applications of metal complexes of Schiff bases-a review. *J Sci Ind Res (India)*. 2009;68:181-187.

5. Abu-Dief AM, Mohamed IM. A review on versatile applications of transition metal complexes incorporating Schiff bases. Beni-Suef Univ. *J Basic Appl Sci*. 2015;4:119-133.

6. Wani AL, Parveen N, Ansari MO, Ahmad MF, Jameel S, Shadab GGHA. Zinc: an element of extensive medical importance. *Curr Med Res Pract*. 2017;7:90-98.

7. Borkert CM, Cox FR, Tucker MR. Zinc and copper toxicity in peanut, soybean, rice, and corn in soil mixtures. *Commun Soil Sci Plant Anal*. 1998;29:2991-3005.

8. Jackson MJ, Lowe NM. Physiological role of zinc. *Food Chem*. 1992;43:233-238.

9. Bartzatt R. Neurological impact of zinc excess and deficiency in vivo. *Eur J Nutr Food Saf*. 2017;7:155-160.

10. Marger L, Schubert CR, Bertrand D. Zinc: an underappreciated modulatory factor of brain function. *Biochem Pharmacol*. 2014;91:426-435.

11. Prasad AS. Zinc deficiency in women, infants and children. *J Am Coll Nutr*. 1996;15:113-120.

12. Bettger WilliamJ, O'Dell BoydL. A critical physiological role of Zinc in the structure and function of biomembranes. *Zinc Biomembr*. 1981;28:1425-1438.

13. Fukada T, Yamasaki S, Nishida K, Murakami M, Hirano T. Zinc homeostasis and signaling in health and diseases. *J Biol Inorg Chem*. 2011;16:1123-1134.

14. Plum LM, Rink L, Hajo H. The essential toxin: impact of zinc on human health. *Int J Environ Res Public Health*. 2010;7:1342-1365.

15. Peng X, Du Jianjun, Fan Jiangli, et al. A selective fluorescent sensor for imaging Cu^{2+} in living cells. *J Am Chem Soc*. 2007;129:1500-1501.

16. Wolfe AJ. The Acetate Switch. *The Acetate Switch Microbiol Mol Biol Rev*. 2005;69:12-50.

17. Pinhal S, Ropers D, Geiselmann J, de JH. Acetate metabolism and the inhibition of bacterial growth by acetate. *J Bacteriol*. 2019;201:e00147-19.

18. Vavere AmyL, Kridel StevenJ, Wheeler FrancesB, JSL. Imaging Fatty Acid Synthase Expression in Prostate Cancer. *J Nucl Med*. 2008;49:327-334.

19. Mei J, Leung NLC, Kwok RTK, Lam JWY, Tang BZ. Aggregation-Induced Emission: together We Shine, United We Soar!. *Chem Rev*. 2015;115:11718-11940.

20. Hong Y, Lam JWY, Tang BZ. Aggregation-induced emission: phenomenon, mechanism and applications. *Chem Commun*. 2009:4332.

21. Jia T-J, Cao W, Zheng X-J, Jin L-P. A turn-on chemosensor based on naphthol–triazole for Al(III) and its application in bioimaging. *Tetrahedron Lett*. 2013;54:3471-3474.

22. Gopikrishna P, Meher N, Iyer PK. Functional 1, 8-Naphthalimide AIE /AIEEgens : recent Advances and Prospects. *ACS Appl Mater Interfaces*. 2018;10:12081-12111.

23. Venkatramaiah N, Kumar GD, Chandrasekaran Y, Ganduri R, Patil S. Efficient Blue and Yellow Organic Light-Emitting Diodes Enabled by Aggregation-Induced Emission. *ACS Appl Mater Interfaces*. 2018;10:3838-3847.

24. Bhalla V, Vij V, Dhir A, Kumar M. Hetero-oligophenylene-Based AIEE Material as a Multiple Probe for Biomolecules and Metal Ions to Construct Logic Circuits: application in. *Chem Eur J*. 2012;18:3765-3772.

25. Dey S, Maity A, Shyamal M, et al. An antipyrine based fluorescence "turn-on" dual sensor for Zn^{2+} and Al^{3+} and its selective fluorescence "turn-off" sensing towards 2,4,6-trinitrophenol (TNP) in the aggregated state. *Photochem Photobiol Sci*. 2019;18:2717-2729.

26. Salinas Y, Martínez-Máñez R, Marcos MD, et al. Optical chemosensors and reagents to detect explosives. *Chem Soc Rev*. 2012;41:1261-1296.

27. Tang W, Xiang Y, Tong A. Salicylaldehyde Azines as Fluorophores of Aggregation-Induced Emission Enhancement Characteristics A series of salicylaldehyde azine derivatives were found to exhibit interesting aggregation-induced emission enhance- ment (AIEE) characteristics . In goo. *J Oranic Chem*. 2009:2163-2166.

28. Li H, Shu H, Liu Y, et al. Aggregation-Induced Emission of Highly Planar Enaminone Derivatives: unexpected Fluorescence Enhancement by Bromine Substitution. *Adv Opt Mater*. 2019;7:1-5.

29. Zhou H, Yang B, Wen G, Hu X, Liu B. Assembly and disassembly activity of two AIEE model compounds and its potential application. *Talanta*. 2018;184:394-403.

30. Ma X, Cheng J, Liu J, Zhou X, Xiang H. Ratiometric fluorescent pH probes based on aggregation-induced emission-active salicylaldehyde azines. *New J Chem*. 2015;39:492-500.

31. Xie DX, Ran ZJ, Jin Z, Zhang XB, An DL. A simple fluorescent probe for Zn(II) based on the aggregation-induced emission. *Dye Pigment*. 2013;96:495-499.

32. Consiglio G, Oliveri IPietro, Failla S, Bella SDi. On the Aggregation and Sensing Properties of Zinc(II) Schiff-Base Complexes of Salen-Type Ligands. *Molecules*. 2019;24(13):2514.

33. Suganyaa S, Velmathia S, Venkatesanb P, Wu S-P, Boobalan MS. Highly Fluorescent Zinc Complex of Dipodal N-Acyl hydrazone as a Selective Sensor for $H_2PO_4^-$ ion and Application in Living Cells. *Inorg Chem Front*. 2015;2:649-656.

34. Zo HJ, Song JY, Lee JJ, Velmathi S, Park JS. Highly selective response of bipyridyl-incorporated acetyelene dye for zinc acetate. *Talanta*. 2013;112:80-84.

35. *SMART (V 5.628), SAINT (V 6.45a). SMART (V 5.628), SAINT (V 6.45a), XPREP, SHELXTL*, Bruker AXS Inc., Madison, WI, 2004.

36. Sheldrick GM. Crystal structure refinement with SHELXL. *Acta Crystallogr Sect C Struct Chem*. 2015;71:3-8.

37. Mabhai S, Dolai M, Dey S, Dhara A, Das B, Jana A. A novel chemosensor based on rhodamine and azobenzene moieties for selective detection of Al^{3+} ion. *New J Chem*. 2018;42:10191-10201.

38. Mistri T, Dolai M, Chakraborty D, Khuda-Bukhsh AR, Das KK, Ali M. A highly selective and sensitive in vivo fluorosensor for zinc(II) without cytotoxicity. *Org Biomol Chem*. 2012;10:2380-2384.

39. Benesi HA, Hildebrand JH. A Spectrophotometric Investigation of the Interaction of Iodine with Aromatic Hydrocarbons. *J Am Chem Soc*. 1949;71:2703-2707.

40. Lakowicz JR. *Principles of Fluorescence Spectroscopy*. New York: Plenum; 1999.

41. Parr RG. Density-Functional Theory of Atoms and Molecules. *Horizons Quantum Chem*. 1980:5-15.

42. Barone V, Cossi M. Conductor Solvent Model. *J Phys Chem A*. 2001;102:1995-2001.

43. Cossi M, Rega N, Scalmani G, Barone V. Energies, structures, and electronic properties of molecules in solution with the C-PCM solvation model. *J Comput Chem*. 2003;24:669-681.

44. Cossi M, Barone V. Time-dependent density functional theory for molecules in liquid solutions. *J Chem Phys*. 2001;115:4708-4717.

45. Becke AD. Density-functional thermochemistry. III. The role of exact exchange. *J Chem Phys*. 1993;98:5648-5652.

46. Lee C, Yang W, Parr RG. Development of the Colle-Salvetti correlation-energy formula into a functional of the electron density. *Phys Rev B*. 1988;37:785-789.

47. Stratmann RE, Scuseria GE, Frisch MJ. An efficient implementation of time-dependent density-functional theory for the calculation of excitation energies of large molecules. *J Chem Phys*. 1998;109:8218-8224.

48. Frisch MJ, Trucks GW, Schlegel HB, et al. *Gaussian 09*. Wallingford CT: Revision D.01. Gaussian Inc.; 2009.

49. O'Boyle NM, Tenderholt AL, Langner KM. CHARMM: the Biomolecular Simulation Program B. *J Comput Chem*. 2008;29:839-845.

50. Safin DA, Robeyns K, Garcia Y. Solid-state thermo- and photochromism in N,N′-bis(5-X-salicylidene) diamines (X = H, Br). *RSC Adv*. 2012;2:11379-11388.

51. Dolai M, Saha U, Das AK, Kumar GS. Single sensors for multiple analytes employing fluorometric differentiation for Cr^{3+} and Al^{3+} in semi-aqueous medium with bio-activity and theoretical aspects. *Anal Methods*. 2018;10:4063-4072.

52. Saha U, Dolai M, Suresh Kumar G. Adaptable sensor for paying fluorometric detection of methanol molecules: theoretical aspects and DNA binding studies. *New J Chem*. 2019;43:8982-8992.

53. Qin J-C, Fan L, Yang Z-Y. A small-molecule and resumable two-photon fluorescent probe for Zn^{2+} based on a coumarin Schiff-base. *Sens Actuators, B*. 2016;228:156-161.

54. Pannipara M, Al-Sehemi AG, Irfan A, Assiri M, Kalam A, Al-Ammari YS. AIE active multianalyte fluorescent probe for the detection of Cu^{2+}, Ni^{2+} and Hg^{2+} ions. *Spectrochim Acta - Part A Mol Biomol Spectrosc*. 2018;201:54-60.

55. Martinho JMG. Heavy-atom quenching of monomer and excimer pyrene fluorescence. *J Phys Chem*. 1989;93:6687-6692.

56. Pandey R, Kumar P, Singh AK, et al. Fluorescent zinc(II) complex exhibiting "on-off-on" switching toward Cu^{2+} and Ag^+ ions. *Inorg Chem*. 2011;50:3189-3197.

57. Paquin F, Rivnay J, Salleo A, Stingelin N, Silva C. Multi-phase semicrystalline microstructures drive exciton dissociation in neat plastic semiconductors. *J Mater Chem C*. 2015;3:10715-10722.

58. Gogoi A, Samanta S, Das G. A benzothiazole containing CHEF based fluorescence turn-ON sensor for Zn^{2+} and Cd^{2+} and subsequent sensing of $H_2PO_4^-$ and $P_4O_7^{4-}$ in physiological pH. *Sensors Actuators, B Chem*. 2014;202:788-794.

59. Du K, Niu S, Qiao L, et al, A highly selective ratiometric fluorescent probe for the cascade detection of Zn^{2+} and $H_2PO_4^-$ and its application in living cell imaging. *RSC Adv*. 2017, 7, 40615-40620.

60. *Guidelines for drinking-water quality, Zinc in Drinking-Water*. WHO 1996 Vol. 2.

61. Wu JS, Liu WM, Zhuang XQ, et al. Fluorescence turn on of coumarin derivatives by metal cations: a new signaling mechanism based on C = N isomerization. *Org Lett*. 2007;9:33-36.

62. De Silva AP, Moody TS, Wright GD. Fluorescent PET (Photoinduced Electron Transfer) sensors as potent analytical tools. *Analyst*. 2009;134:2385-2393.

63. Santra S, Krishnamoorthy G, Dogra SK. Excited-state intramolecular proton transfer in 2-(2′-Acetamidophenyl)benzimidazole. *J Phys Chem A*. 2000;104:476-482.

64. Abou-Zied OK, Jimenez R, Thompson EHZ, Millar DP, Romesberg FE. Solvent-dependent photoinduced tautomerization of 2-(2′-hydroxyphenyl)benzoxazole. *J Phys Chem A*. 2002;106:3665-3672.

65. Kim J, Kim S, Park SY, Joo T. Excited State Intramolecular Proton Transfer Dynamics of Oxadiazole-based Dyes. *Bull Korean Chem Soc*. 2015;36:855-861.

66. Shahid M, Misra A. Photoenolization via excited state proton transfer and ion sensing studies of hydroxy imidazole derivatives. *J Photochem Photobiol A Chem*. 2017;335:190-199.

67. Jana A, Das B, Mandal SK, Mabhai S, Khuda-Bukhsh AR, Dey S. Deciphering the CHEF-PET-ESIPT liaison mechanism in a Zn^{2+} chemosensor and its applications in cell imaging study. *New J Chem*. 2016;40:5976-5984.

68. Bhalla V, Roopa; Kumar M. Fluoride triggered fluorescence "turn on" sensor for Zn^{2+} ions based on pentaquinone scaffold that works as a molecular keypad lock. *Org Lett*. 2012;14:2802-2805.

69. Dong Y, Li J, Jiang X, Song F, Cheng Y. Naþ Triggered Fluorescence Sensors for Mg^{2+} Detection Based on a Coumarin Salen Moiety. *Org Lett*. 2011;13:2252-2255.

70. Wang J, Miao X, Fengzhao Q, Ren C, Yang Z, Wang L. Enzymatic and reductive triggered hydrogelation of peptide-based gelators combined with alginate gel. *Anal Methods*. 2013(5):5584-5588.

71. Jin CC, Fukuda M, Wu C, et al. A pyrene-armed hexahomotrioxacalix[3]arene as a multi-sensor via synergistic and demetallation effects. *Tetrahedron*. 2015;71:9593-9597.

72. Kowser Z, Rayhan U, Rahman S, Georghiou PE, Yamato T. A fluorescence "turn-on" sensor for multiple analytes: oAc⁻ and F⁻ triggered fluorogenic detection of Zn^{2+} in a co-operative fashion. *Tetrahedron*. 2017;73:5418-5424.

SUPPORTING INFORMATION

Additional supporting information may be found online in the Supporting Information section at the end of the article.